

Preclinical Testing of a Novel Niclosamide Stearate Prodrug Therapeutic (NSPT) Shows Efficacy Against Osteosarcoma

Gireesh B. Reddy¹, David L. Kerr², Ivan Spasojevic^{3,4}, Artak Tovmasyan³, David S. Hsu^{3,4}, Brian E. Brigman^{2,3}, Jason A. Somarelli^{3,4}, David Needham^{3,5,6}, and William C. Eward^{2,3}



ABSTRACT

Therapeutic advances for osteosarcoma have stagnated over the past several decades, leading to an unmet clinical need for patients. The purpose of this study was to develop a novel therapy for osteosarcoma by reformulating and validating niclosamide, an established anthelmintic agent, as a niclosamide stearate prodrug therapeutic (NSPT). We sought to improve the low and inefficient clinical bioavailability of oral dosing, especially for the relatively hydrophobic classes of anticancer drugs. Nanoparticles were fabricated by rapid solvent shifting and verified using dynamic light scattering and UV-vis spectrophotometry. NSPT efficacy was then studied *in vitro* for cell viability, cell proliferation, and intracellular signaling by Western blot analysis; *ex vivo* pulmonary metastatic assay model; and *in vivo* pharmacokinetic and lung mouse metastatic model of osteosarcoma. NSPT formulation stabilizes niclosamide stearate

against hydrolysis and delays enzymolysis; increases circulation *in vivo* with $t_{1/2}$ approximately 5 hours; reduces cell viability and cell proliferation in human and canine osteosarcoma cells *in vitro* at 0.2–2 $\mu\text{mol/L}$ IC_{50} ; inhibits recognized growth pathways and induces apoptosis at 20 $\mu\text{mol/L}$; eliminates metastatic lesions in the *ex vivo* lung metastatic model; and when injected intravenously at 50 mg/kg weekly, it prevents metastatic spread in the lungs in a mouse model of osteosarcoma over 30 days. In conclusion, niclosamide was optimized for preclinical drug delivery as a unique prodrug nanoparticle injected intravenously at 50 mg/kg (1.9 mmol/L). This increased bioavailability of niclosamide in the blood stream prevented metastatic disease in the mouse. This chemotherapeutic strategy is now ready for canine trials, and if successful, will be targeted for human trials in patients with osteosarcoma.

Introduction

Osteosarcoma has seen almost no chemotherapeutic advances over the past 3 decades

Osteosarcoma is the most common primary bone malignancy in humans. It most frequently occurs in adolescence (1). At presentation, 15%–20% of patients already have visible pulmonary metastatic disease, and a majority of patients have lung metastases that are not yet detectable (2). Because most patients without visible metastatic disease at presentation likely have undetectable micrometastasis, systemic therapy, both neoadjuvant and adjuvant therapy, is a critical addition to surgical resection (3). Sadly, osteosarcoma, unlike most other solid tumors, has seen relatively few chemotherapeutic advances over the past 3 decades, particularly with respect to patients presenting with advanced or metastatic disease (4–8). Indeed, osteosarcoma is one

of the only types of cancer for which the prognosis given today is nearly identical to the prognosis given in 1988 (9). Furthermore, the standard-of-care chemotherapy regimen of methotrexate, Adriamycin (doxorubicin), and cisplatin is based on cytotoxic agents associated with substantial treatment-derived morbidity (10–12). Although chemotherapeutic sequela can prematurely delay or abort treatment regimens in pediatric and adolescent patients, more severe complications such as anthracycline-induced cardiomyopathy greatly increase subsequent morbidity (2, 13). Indeed, even osteosarcoma survivors do not have a normal life expectancy due to the morbidity from their adolescent therapy. Given the extensive toxicity of these agents, there is a critical need to identify new therapeutics with lower systemic toxicity and greater efficacy to treat osteosarcoma with better outcomes and less treatment-derived morbidity.

Repurposing niclosamide for anticancer applications

Since around 2010, there has been a steady rise in popularity of studies investigating niclosamide for a range of diseases, including Parkinson, diabetes, bacterial and viral infections, and cancer (14). Niclosamide, an FDA-approved anthelmintic, has recently attracted considerable interest as a novel antitumor agent (15–20). Pharmacologically, niclosamide has been shown to be a very “dirty” drug; it inhibits (at least) 17 different pathways in cancer cells (18, 21). In the context of osteosarcoma, niclosamide inhibits multiple pathways that promote survival and growth that are known to be dysregulated in osteosarcoma, including the Wnt/ β -catenin, Akt/mTOR/PI3K, JAK/STAT, NOTCH, and NF- κ B pathways (15, 21–24).

In vitro studies have shown that niclosamide induces cell-cycle arrest in G_1 – G_0 -phase with cell viability IC_{50} s in the 100s of nmol/L to low $\mu\text{mol/L}$ range (25–27). In fact, *in vitro* studies of niclosamide with the NCI-60 human cancer cell lines indicate that niclosamide inhibits cell growth in all tested cancer cell lines (28). In osteosarcoma,

¹Duke University School of Medicine, Durham, North Carolina. ²Department of Orthopaedic Surgery, Duke University Medical Center, Durham, North Carolina. ³Duke Cancer Institute, Durham, North Carolina. ⁴Department of Medicine, Duke University, Durham, North Carolina. ⁵Department of Mechanical Engineering and Material Science, Duke University, Durham, North Carolina. ⁶School of Pharmacy, University of Nottingham, Nottingham, United Kingdom.

Note: Supplementary data for this article are available at Molecular Cancer Therapeutics Online (<http://mct.aacrjournals.org/>).

G.B. Reddy and D.L. Kerr contributed equally as co-first authors of this article.

Corresponding Author: William C. Eward, Duke Medical Center, Box 91006, Durham, NC 27708. Phone: 919-667-6963; Fax: 919-681-7645; E-mail: william.eward@duke.edu

Mol Cancer Ther 2020;19:1448–61

doi: 10.1158/1535-7163.MCT-19-0689

©2020 American Association for Cancer Research.

niclosamide also inhibits cell-cycle progression, and one of its main mechanisms of cell death seems to be induction of apoptosis (29–32). With limited formulations for preclinical evaluation, few studies have been conducted with this drug against cancer *in vivo*. Importantly, although in direct contrast to conventional chemotherapies, *in vitro*, niclosamide is relatively nontoxic to healthy cells, including fibroblasts, normal mammary epithelial cells (MCF-10A), and peripheral blood mononuclear cells, and shows no evidence of causing developmental toxicity, mutagenicity, or carcinogenicity when taken orally (16, 33). Indeed, few, if any, anticancer compounds exhibit such a low-toxicity/high-efficacy profile and hit so many different cell targets.

Inefficient clinical bioavailability of oral dosing

One of the most important problems in drug delivery to tumors remains is the low and inefficient clinical bioavailability of oral dosing, especially for the many hydrophobic classes of anticancer drugs. This is compounded by the fact that there is a dearth of truly effective formulation options, even for preclinical validation that provide high plasma concentration dosing. What is needed for any preclinical validation is an intravenously injectable formulation that puts considerable bioavailable amounts of such drugs in the circulation. Only then can the highly insoluble drug (in our case niclosamide) reach the cancer cells by one or more of several mechanisms and have its intended effects *in vivo*.

For example, in its anthelmintic application, niclosamide is taken orally at doses as much as 2 g per patient (veterinary or human) and has median lethal dose (LD₅₀) values of >1,000 mg/kg (toxicity category III, slightly toxic and slightly irritating; ref. 34). Niclosamide is a Biopharmaceutical Classification System (BCS) class II drug, meaning it has poor water solubility (4 $\mu\text{mol/L}$ at pH 7.4) and its intestinal absorption is rate limited by dissolution (35). Because of this inherently poor aqueous solubility, niclosamide has an extremely low systemic bioavailability in the blood stream and thus has extremely low bioavailability that hampers its repurposing in cancer.

Experience with its oral formulation for worms and consideration of its physicochemical properties (logP 4.5; Sw 4 $\mu\text{mol/L}$) suggests that, in its current tablet formulation, it is actually not suitable for clinical administration for cancer to achieve efficacious results. Indeed, in a recent human prostate cancer clinical trial, the short-lived plasma concentrations that were achieved at the maximum oral dosing (500 mg given three times daily) were only in the range, 35.7–82 ng/mL (0.1–0.25 $\mu\text{mol/L}$; ref. 36). These values, which were only approximately 0.014% of the ingested dose, were below the therapeutic threshold of 0.5 $\mu\text{mol/L}$ for colony formation, as measured for LNCaP prostate cancer cell studies *in vitro* (37). Clinically, there were no PSA declines in any enrolled subject and the Data Safety Monitoring Board closed the study for futility. Similarly, in a new on-going clinical phase I study in patients with resectable colon cancer, niclosamide is still being given as the low-bioavailability oral formulation; it is likely to be a very successful phase I toxicity study, but, in view of the earlier prostate cancer clinical trial, efficacy may well be compromised (36, 38). Finally, early results reported in a very recent American Society of Clinical Oncology abstract of a prospective phase II clinical trial of niclosamide in patients with metastasized colorectal cancer (mCRC) progressing under standard therapy (NIKOLO) indicate that an oral dosing of 2 g per patient can achieve median C_{max} plasma levels of 0.665 $\mu\text{g/mL}$ ($\sim 2 \mu\text{mol/L}$; ref. 39, 40). While encouraging, these are still relatively modest levels that are comparable only with IC₅₀s for cell viability. Importantly, no drug-related toxicities were observed. Thus, the biggest challenge for repurposing niclosamide for cancer is not toxicity, but delivery. The drug must be made more bioavailable in the blood

stream and have a more effective pharmacokinetic profile, including higher plasma bioavailability concentration and circulation half-life.

Reformulation of niclosamide as a niclosamide stearate prodrug therapeutic

Because all clinical niclosamide has only been dosed orally, the MTD has never been determined by intravenous administration directly to the blood stream. Thus, we sought to identify the intravenous injectable MTD and determine what doses of niclosamide could be directly delivered to cancer cells to improve efficacy in early-stage metastatic disease. To do this, we have formulated niclosamide as new niclosamide stearate prodrug therapeutic (NSPT; refs. 41–44). Using this nanoparticle formulation, we have started to address some of the main issues of how to increase the bioavailability of BCS class II and IV anticancer drugs and enable effective validation in preclinical studies, and for subsequent canine and human clinical trials (45, 46).

Current alternative formulations of niclosamide in preclinical development may be hampered by low percent loading (particularly in micelle and many polymer particles), low dosing, low *in vivo* bioavailability, and inefficient access to the tumor interstitium due to large particle size when tested *in vivo* (refs. 32, 47–55; Supplementary Data S1.5). To avoid the low bioavailability route of oral uptake and to improve on existing formulations hindered by the above limitations, nanoparticles are needed that (i) enable direct intravenous injection to increase bioavailability and (ii) deliver more drug per particle into the blood stream. The “bottom-up” design approach for creating a pure-drug-cored nanoparticle using a less water soluble form of niclosamide and rapid solvent exchange thus achieves the above goals and allows for the production of stabilized prodrug nanoparticles (35, 44, 56–58).

Materials and Methods

Materials

NSPTs were created using the following materials and manufacturers: niclosamide stearate was synthesized by the Duke Small Molecule Synthesis Facility (<https://sites.duke.edu/smsf/facility-over-view/>); niclosamide anhydrous (Sigma Aldrich), chloroform stock solutions (DSPC, cholesterol, and DSPE PEG²⁰⁰⁰; Avanti Polar Lipids, Inc.), acetone ($\geq 99.8\%$; Sigma Aldrich), absolute ethanol ($\geq 99.8\%$; VWR Chemicals), chloroform (Rathburn Chemicals Ltd.), buffer solution components (hydrochloric acid, sodium chloride, and sodium hydroxide; VWR Chemicals), acetic acid (Fluka), sodium phosphate monobasic (Sigma Aldrich), and Millipure water.

Preparation of NSPTs

As described by Walke and colleagues and Hervella and colleagues, the NSPT nanoparticles were made by adapting a rapid solvent exchange method to a new prodrug, niclosamide stearate (41–44, 56, 57). In this method, an organic solution of niclosamide stearate and lipids (DSPC, cholesterol, and DSPE-PEG²⁰⁰⁰ in a 45:50:5 ratio) were mixed in a 1:1 equivalent molar ratio in acetone-ethanol and rapidly injected into an excess antisolvent of ultrapure water. Following classical nucleation theory, rapid precipitation spontaneously generates nanoparticles consisting of a core of niclosamide stearate coated with a monolayer of the lipids suspended in a mainly aqueous phase, containing 10% of the initial acetone-ethanol solvents (41–44, 59). The size of particles (hydrodynamic diameter) was measured using a Dynamic Light Scattering Instrument (Dyna Pro Nanostar, Wyatt Technology). The NSPT suspension was stored at 4°C until use. The concentration prior to use was verified

Reddy et al.

using UV Spectrophotometry (SpectraMax, Molecular Devices) by measuring the calibrated absorbance of niclosamide-stearate at 330 nm (see Supplementary Data S2.2 for detailed low- and high-dosing protocols).

***In vitro* stability of NSPT in PBS and plasma**

The chemical stability of NSPT, that is, hydrolysis of niclosamide stearate to produce niclosamide was investigated by 37 °C incubation of 1.8 mmol/L NSPT in (i) PBS, (ii) mouse, and (iii) human plasma. A set of three aliquots per timepoint of each medium was prepared on ice, placed into preequilibrated rack/water bath in 37 °C incubator, and aliquots were taken from incubator and placed on dry ice at: 1 minute (“zero”), 15 minutes, 30 minutes, 1 hour, 2 hours, 4 hours, 8 hours, and 24 hours. Concentration of both niclosamide stearate and niclosamide were measured by high-performance liquid chromatography (HPLC) as described below.

Pharmacokinetics of NSPTs

Analysis of chemical composition was performed by HPLC for niclosamide and niclosamide stearate up to 24 hours after incubation in PBS buffer, mouse and human plasma, and serially drawn blood samples from inoculated mice (Supplementary Data S2.4.1 and S2.4.2). Pharmacokinetic parameters (e.g., C_{max} , t_{max} , $t_{1/2}$, and AUC) were calculated by noncompartmental approach within WinNonlin Software (Pharsight Inc.).

Cell culture

Human osteosarcoma 143B, U2OS, MG63, and SAOS2 cells were obtained from the Duke Cell Culture Facility, which performs routine *Mycoplasma* testing and verifies cell identity by analysis of short tandem repeats. Canine osteosarcoma Abram's, D17, and Moresco cell lines were provided courtesy of Dr. Doug Thamm (V.M.D. Colorado State University, Fort Collins, CO). The canine osteosarcoma D418 cell line was developed from a canine osteosarcoma patient-derived xenograft (PDX, Somarelli, Altunel and colleagues unpublished). The 143B, MG-63, D418, Abrams, D17, and Moresco cells were cultured in standard DMEM (Thermo Fisher Scientific) and the U2OS and SAOS2 lines in McCoy's 5A Modified Medium (Thermo Fisher Scientific). Cells were passed every 2–4 days and were not allowed to reach full confluence.

Dose–response assays of NSPTs on canine osteosarcoma growth

Dose-dependent effects of NSPTs on all human and canine osteosarcoma cell lines' growth were determined using a dose–response CellTiter Glo Assay (Promega Corporation). To do this, 2,500 cells were seeded per well in flat-bottomed 96-well plates. Media (100 μ L) containing either niclosamide in DMSO or NSPTs was added at increasing concentrations (1.6 nmol/L, 8 nmol/L, 40 nmol/L, 200 nmol/L, 1 μ mol/L, 5 μ mol/L, 25 μ mol/L, and 100 μ mol/L). Data were compared with a buffer (no drug) control. Cells were incubated at 37 °C for 72 hours and then their cell viability was assessed using the CellTiter Glo Substrate Metabolic End-point Assay (Promega) by addition of 50 μ L/well of the CellTiter Glo substrate. Luminescence was measured with SpectraMax M-series Microplate Reader (Molecular Devices). Signal was normalized to the average of untreated (PBS control) wells.

Western blot analysis of canine cell lines

The ability of NSPTs to modulate signaling pathways known to be dysregulated in osteosarcoma was investigated by Western blotting. A

total of 3×10^5 cells/well of the human osteosarcoma cell line 143B and patient-derived canine xenograft (D418) cell line were plated and subsequently incubated with a concentration of niclosamide or NSPTs that were known, from the viability assays, to be on the order of the amount required to reduce cell viability to almost zero. As shown in the results of the cell viability assay (shown later in Fig. 3) this value was at least 20 μ mol/L niclosamide or NSPT. Cells were therefore incubated for 0, 1, 2, 4, and 8 hours with 20 μ mol/L niclosamide or NSPT. Cytosolic and nuclear fractions of lysates at intermediate timepoints were extracted with RIPA lysis buffer and the Nuclear/Cytoplasmic Extraction Reagent (NE-PER, Thermo Fisher Scientific). Halt protease and phosphatase inhibitor cocktail were added to both lysis buffers for a final concentration of $2 \times$. Cell lysates were centrifuged at $16,000 \times g$ at 4 °C for 15 minutes. Lysate was separated via Nu PAGE 4%–12% Bis-Tris SDS-PAGE and transferred onto nitrocellulose membranes. After blocking with Superblock (TBS) Blocking Buffer (Thermo Fisher Scientific), membranes were incubated with primary antibody overnight at 4 °C and secondary antibody for 1 hour at room temperature. Primary antibodies included anti-pS6 ser235/236 (clone 91B2, 1:1,000), anti-S6 (clone 54D2, 1:1,000), anti-Notch1 (clone D1E11, 1:1,000), anti-Akt (pan) (clone 11E7, 1:1,000), anti-pSTAT3 tyr705 (clone D3A7, 1:2,000), anti-Histone H3 (clone D1H2, 1:2,000), anti- β -catenin (clone L87A12, 1:1,000), anti-pAkt Ser473 (clone 193H12, 1:1,000), and anti-STAT3 (clone 123H6, 1:1,000, Cell Signaling Technology). Loading controls included anti-GAPDH (1:5,000, Abcam) and anti-alpha tubulin (1:5,000, Abcam). IRDye 680 nm and 800 nm secondary antibodies were purchased from LI-COR. Western blots were imaged with the Odyssey Fc Imaging System and analyzed using Image Studio Software (LI-COR). Signal was normalized to GAPDH, α -tubulin, or Histone H3 loading controls.

Isolation of NLS mCherry-labeled human and canine osteosarcoma clones

Nuclear localizing signal (NLS) mCherry-labeled 143B human and D418 canine osteosarcoma cell reporters were isolated for *in vitro* multiplexed measurements of the effects of NSPTs on osteosarcoma proliferation and apoptosis. Cells were treated with NSPT at the following concentrations: 1.6 nmol/L, 8 nmol/L, 40 nmol/L, 200 nmol/L, 1 μ mol/L, 5 μ mol/L, 25 μ mol/L, and 100 μ mol/L. NLS mCherry lentiviral vectors were constructed by the Viral Vector Core, Duke University School of Medicine (Durham, NC). Time- and dose–response assays of NSPTs on NLS mCherry-labeled 143B human and D418 canine osteosarcoma cells, representing phase confluence %, used red object fluorescence for cell count and green object fluorescence for cell area. Osteosarcoma cell lines were plated at 3×10^5 cells/well onto 6-well plates. Cells were incubated with viral titer (multiplicity of infection of 5) and polybrene (1:500) for 12 hours. NLS mCherry osteosarcoma cell lines were then FACS sorted on a MoFlo Astrios EQ (Beckman Coulter) sorter using Summit Software (Cytomation). Nontransduced lines were used to determine the fluorescence gating strategy. The top 50% of NLS mCherry cells were then sorted and a post-sort analysis confirmed purity.

Live cell imaging for kinetic determination of proliferation and analysis of apoptosis

Live cell imaging assessment of NSPTs' effects on NLS mCherry-labeled human and canine osteosarcoma proliferation and apoptosis were performed using the IncuCyte S3 (Essen BioScience) with the DEVD-amino acid (Asp-Glu-Val-Asp motif) substrate (IncuCyte Caspase-3/7 Green Apoptosis Assay Reagent, Essen BioScience). Cells were treated with the same concentrations of NSPTs (1.6 nmol/L, 8 nmol/L, 40 nmol/L, 200 nmol/L, 1 μ mol/L, 5 μ mol/L, 25 μ mol/L, and

100 $\mu\text{mol/L}$) for 72 hours. Phase contrast red and green fluorescence channel images were acquired every 2 hours. IncuCyte S3 imaging software was utilized to calculate percent confluency, total NLS cell red fluorescence area per well, and total caspase green fluorescence area. Images were assessed for final plots at 96 hours.

Generation of zsGreen-labeled human and canine osteosarcoma clones for pulmonary metastasis assay

To label osteosarcoma cells with zsGreen, a total of 3×10^5 HEK293T cells were plated onto 6-well plates in complete DMEM and transfected using Lipofectamine LTX plus at 30% confluence with a vector-mix consisting of 2.0 μg pCL-Ampho, and 2.0 μg pLCNX2 zsGreen construct DNA (CloneTech). Human and canine osteosarcoma cell lines were plated at 3×10^5 cells/well onto 6-well plates. Viral supernatant was collected off HEK293T cells and transferred onto adherent mid-log human and canine osteosarcoma cells using a 0.40- μm CA filter. Transduced human and canine osteosarcoma cell lines were selected with 100 $\mu\text{g/mL}$ G418 for 14 days.

Ex vivo pulmonary metastasis assay

The *ex vivo* pulmonary metastasis assay (PuMA) was utilized as described previously (60, 61) to assess the efficacy of NSPTs to inhibit the growth of zsGreen-labeled human (143B) and canine (D418) osteosarcoma cells in the metastatic pulmonary tumor microenvironment (See Supplementary Data for full description).

Determination of NSPT maximum tolerable dose

We attempted to determine the single maximal tolerable dose (sMTD) of NSPT for the intravenous route (via tail-vein injection). We carried out a step-wise dose increase with one mouse at the lowest dose and 3 mice per higher doses until any significant impact on mouse behavior was observed over 24 hours. C57BL/6 mice (Jackson Laboratory) were injected with a volume of 0.1 or 0.2 or 0.25 mL per dose. At the time of this study, we had not observed any toxicity with an injection of 200 μL (0.2 mL) of a 100 $\mu\text{mol/L}$ concentrated suspension of NSPTs, and so 1 mmol/L NSPT was selected to be the starting injected dose. Again, at the time, the highest achievable dose of the NSPT preparation was 6 mmol/L, and so single 0.1 mL injections of 1 and 6 mmol/L NSPT were administered to give approximate dosing of 3 and 20 mg/kg, respectively. Higher target doses of 36 and 47 mg/kg were achieved by increasing the volume of injection of the 6 mmol/L suspension to 0.2 mL and 0.25 mL, respectively. A single intravenous dose of NSPT that did not cause significant behavioral change in behavior of all 3 mice was considered tolerated. As shown in Results, the highest dose was well-tolerated and so this dosing did not actually achieve a sMTD.

Generation of luciferase-labeled human and canine osteosarcoma clones

To measure lung colonization and metastatic tumor growth and development, *in vivo*, in the metastatic mouse model over time, we generated luciferase-labeled human and canine osteosarcoma clone reporters. These reporter cells provided an accurate and accessible assessment of *in vivo* metastatic tumor burden when animals were administered the luciferin substrate and viewed by an *In Vivo* Imaging System (Caliper Life Sciences, Inc., PerkinElmer). Lentiviral transduction of a luciferase-expressing plasmid was carried out as described above for zsGreen labeling. PCW-107 was a gift from Dr. Kris Wood, PhD, Duke University, Durham, NC. Equivalent luciferase-expressing clones were selected via the Dual-Luciferase Reporter Assay System (Promega).

Mouse studies of osteosarcoma metastasis at two NSPT dosing levels

Osteosarcoma tail-vein metastasis studies were carried out at two NSPT dosing levels of 0.59 and 50 mg/kg. Luciferase-labeled osteosarcoma cell lines 143B (Human) and D418 (canine patient derived) were cultured as described above. Cells were harvested for injection by trypsinization while in mid-log phase of growth (50%–80% confluence) and concentrated to 5×10^6 cells/mL in Dulbecco's PBS. Viability was assessed to be >90% by hemocytometer prior to inoculation. Cells were kept at 4°C until inoculation, which occurred within 2 hours of preparation. Animal studies were performed in accordance with the approved protocols of the Duke University Institutional Animal Care and Use Committee (Durham, NC).

In this lung metastasis model, cells were injected by tail-vein injection on "day 0" and allowed to reach and start to colonize the lungs for 1 day before NSPT nanoparticles were administered intravenously again by tail-vein injection. The model, therefore, allowed for direct exposure of osteosarcoma cancer cells that were in the very first and early stages of lung colonization. These cells were thus likely to be accessible from the blood stream by the intravenous injection of each 200 μL dose of nanoparticles (0.59 or 50 mg/kg). Controls were the same volume of PBS (200 μL) and an intraperitoneal injection of doxorubicin, 1.2 mg/kg in PBS. Thus, on "day 0," the osteosarcoma cell preparations (1×10^6 cells in 200 μL PBS) were injected directly into the tail veins of 6-week-old SCID (Prkdc^{scid}) and beige (Lyst^{bg}) mice (Charles River Laboratories), approximately 20 g in weight. Then, starting on "day 1" post-inoculation, mice underwent randomized stratification on the basis of initial pulmonary seeding luminescence and sex. The total number of mice was 50, consisting of 5 mice in each group. Mice were randomly distributed among the following treatment groups: PBS, NSPT, doxorubicin (low- and high-dose groupings in Supplementary Data S2.14.1).

Mice were weighed every 3 days and monitored for signs of morbidity as evidence of presumed pulmonary metastases or side effects of treatment. Signs monitored included anorexia, dehydration, dyspnea, diarrhea, lethargy, or decreased grooming activity. To produce the tumor cell luminescence, prior to imaging, mice were injected intraperitoneally with D-Luciferin in 200 μL PBS (GoldBio) at 150 mg/kg. To determine time-to-peak luminescence, a kinetic determination of D-Luciferin biodistribution was carried out by serial imaging mice with known pulmonary disease for 30 minutes following luciferin injection. Results (Supplementary Fig. S5) showed that peak luminescence was obtained within 15 minutes. Thus, for all subsequent studies, mice were imaged after 15 minutes and the bioluminescence was captured using the IVIS Lumina XR System (Caliper Life Sciences, Inc., PerkinElmer). Living Image 4.5 Software (Caliper) was used to capture the images and quantify the signal. After mice were euthanized, the thoracic cavities were opened and lungs were perfused with 10% buffered formalin by tracheal injection using a blunt perfusion cannula. Lungs were weighed and examined grossly for the number of visible metastatic lesions on the surface and the left lungs were examined histologically for the number of internal metastases by sectioning and microscopic examination after hematoxylin and eosin staining. Ten nonsequential serial sections were examined per animal.

Statistical analysis

Results are displayed as mean \pm SEM, unless otherwise indicated. Luminescence data for the CellTiter Glo assay that measured ATP and hence cell viability in dose-response experiments, were plotted on a log[concentration] scale and fitted with 4-parameter

Reddy et al.

logistic curves, IC_{50} values and SEs were calculated from the curve inflection points. In the 4-parameter logistic model (62), the relationship between the concentration of the drug or prodrug (x) and the cell viability (y), is given by the equation that includes the “4 parameters”:

$$x = c \left(\frac{a - d}{y - d} - 1 \right) \quad (A)$$

a = the minimum value that can be obtained (i.e., what happens at 0 dose).

d = the maximum value that can be obtained (i.e., what happens at infinite dose).

c = the point of inflection (i.e., the point on the S-shaped curve halfway between a and d).

b = Hill's slope of the curve (i.e., this is related to the steepness of the curve at point c).

One-way ANOVA with Tukey *post hoc* multiple comparisons was utilized for pairwise comparisons of PuMA lung tumor burden. Wilcoxon pairwise tests were used to compare *in vivo* bioluminescence data. Statistical analyses for data analyses were performed with JMP Pro (SAS) with a significance level at $P < 0.05$, unless otherwise indicated. Graphs were plotted on Prism 7 (GraphPad).

Results

Size and stability of NSPTs *in vitro* and pharmacokinetics/stability *in vivo*

NSPTs were made for both *in vitro* and *in vivo* studies using the established methods of Hervella and colleagues (41). All formulations were evaluated for size stability in water, and also in nonionic media including, equiosmotic sucrose or glucose, and isotonic PBS. Results showed that all NSPT suspensions, as made, were size stable at 4°C in water, and also in the nonionic equiosmotic sucrose or glucose or PBS (See Supplementary Fig. S1A and S1B; Supplementary Data). The rapid solvent injection method gave a suspension concentration of 100 $\mu\text{mol/L}$ for the low-dose sample, and the nanoparticle size (diameter), directly after making, was measured by DLS (intensity mode) to be 30 ± 5 nm, in close agreement with Hervella and colleagues' results (41). For the up-concentrated sample, the sizes increased slightly. For all five of the 50 mg/kg treatments the “intensity” average distribution particle diameter was 45 ± 5 nm. As shown in Fig. 1A, the intensity average distribution for treatment 1 was $44.7 \text{ nm} \pm 1.6 \text{ nm}$. Shown in Fig. 1B is a scaled schematic of a representative 30 nm diameter NSPT. It is shown with a 16.6 nm diameter, isotropic, core of niclosamide stearate, and a stabilizing lipid monolayer of DSPC:cholesterol, containing a coverage of polyethylene glycol (PEG) provided by 5 mol% of DSPE-PEG²⁰⁰⁰. Detailed discussion of this schematic with reference to its critical size and phase state is reserved for the Discussion section.

The niclosamide stearate is a niclosamide prodrug, in which a fatty acid stearate is covalently linked to niclosamide by an ester bond. *In vivo*, the ester bond is expected to be hydrolyzed by chemical and/or enzymatic hydrolysis, releasing “free” niclosamide. To assess the extent of the hydrolysis and the achieved levels of niclosamide in plasma, we performed a pharmacokinetic experiment in mouse, where 50 mg/kg NSPT was injected intravenously and plasma collected in time within 24 hours. In addition, to learn about the intrinsic stability of NSPT in solution and plasma and to better understand the obtained pharmacokinetic data, 37°C incubation of NSPT in PBS, mouse plasma, and human plasma was performed as well.

The Fig. 2B shows the pharmacokinetic profiles for NSPT (measured as niclosamide stearate) and niclosamide (NIC), both exhibiting single exponential decay of the same half-life ($t_{1/2} = 5$ hours), as calculated from the slope in the log-lin plot (Fig. 2B, inset). Dashed line shows the published data obtained after intravenous bolus administration of niclosamide to rat (63). In this experiment by Chang and colleagues, the compound was administered intravenously at a dose of 2 mg/kg (63). The dosing solution was prepared by dissolving the compound in a mixture of DMSO/cremophor EL/water (3/15/82 v/v/v). Interestingly, compared with the AUCs for our niclosamide stearate of $3,560 \text{ h}^* \mu\text{g/mL}$ and niclosamide of $690 \text{ h}^* \mu\text{g/mL}$, Chang and colleagues showed an AUC of only $1.4 \text{ h}^* \mu\text{g/mL}$ (2,543 times lower than the niclosamide stearate AUC; ref. 63). The inset shows the log-linear plot giving a similar half-life for both niclosamide stearate (5 hours) and niclosamide (5.5 hours) by a single-order decay, and for comparison with our study, we see that Chang and colleagues' direct injection has a similar half-life of 5.7 hours albeit at much lower plasma levels (63).

We dose adjusted and plotted the data to illustrate the magnitude of the gain in niclosamide exposure (AUC) when niclosamide is administered not in its free form but rather as NSPT ($AUC_{\text{NSPT} \rightarrow \text{NIC}}/AUC_{\text{free NIC}} = 470$). The NSPT and niclosamide are of different size and physical properties, so the observed pharmacokinetic profile of the released niclosamide in plasma may be explained as being rate controlled by the rate of NSPT loss from circulation (as observed from similar nanoparticles, $t_{1/2} \sim 7$ hours; ref. 64), whereas the magnitude of the niclosamide plasma concentration is determined by the rate of niclosamide production from NSPT by enzymolysis. Indeed, Fig. 2A shows the *in vitro* production of niclosamide by a mixed order enzymolysis process (fast first order followed by slower zero order) in mouse plasma as being of the same order of magnitude, $t_{1/2}$ ranging from 2 to 13 hours. Figure 2A also reveals that the rate of enzymolysis in human plasma is very similar as in mouse plasma, whereas the simple pH-dependent hydrolysis in aqueous solution (PBS) is much slower as expected for lipid monolayer-protected NSPT core.

Cell viability, proliferation, and ATP present in human and canine osteosarcoma cells *in vitro*

NSPTs inhibited cell viability, proliferation, and the quantity of intracellular ATP present in human and canine osteosarcoma cells *in vitro*. As shown in Fig. 3A for the human 143B and canine D418 cell lines, dose–response assays demonstrated that both niclosamide (from DMSO) and NSPTs (added as an aqueous suspension) inhibited *in vitro* canine and human osteosarcoma cell growth in a dose-dependent manner (See Supplementary Fig. S2A for individual plots of all eight cell lines). Also, the dose response for cell viability gave very similar profiles for both the parent drug niclosamide and the NSPT nanoparticles for both the canine and human cells.

Cumulated in Fig. 3B, IC_{50} values for all cell lines were in the micromolar to sub-micromolar range, showing, in general, that all cells were slightly more sensitive to niclosamide from DMSO when compared with NSPTs (mean IC_{50} : $0.57 \mu\text{mol/L}$ vs. mean IC_{50} : $1.22 \mu\text{mol/L}$, respectively; $P = 0.002$). However, on average, there were no statistically significant differences between inhibition of human and canine osteosarcoma cells by niclosamide and NSPTs (mean IC_{50} : $1.16 \mu\text{mol/L}$ vs. mean IC_{50} : $1.27 \mu\text{mol/L}$, respectively; $P = 0.79$).

Figure 3C shows time- and dose–response assays of NSPTs in terms of a proliferation assay based on NLS mCherry-labeled 143B human

Novel Nanoparticle Niclosamide Treats Osteosarcoma

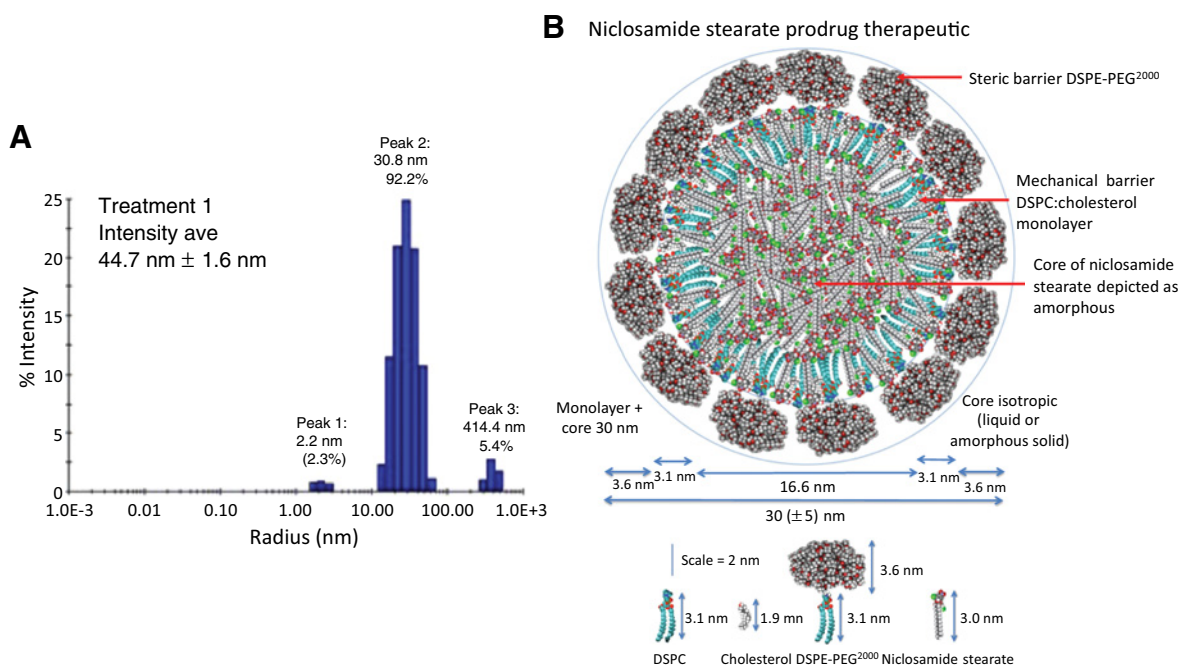


Figure 1.

Nanoparticle size and the composition and structure of the NSPT. **A**, Diameters of nanoparticles measured by DLS directly after making using the rapid solvent injection method. The particle size (hydrodynamic diameter) was measured using a Dynamic Light Scattering instrument (Dyna Pro Nanostar, Wyatt Technology). For all five of the 50 mg/kg treatments, was 45 ± 5 nm. As shown, the DLS algorithm reports three peaks with % intensity values: peak 1: 2.2 nm (2.3%); peak 2: 30.8 nm (92.2%); and peak 3: 414.4 nm (5.4%). Mean polydispersity index (PDI) for treatment 1 was 0.303. Shown is the DLS intensity distribution for treatment 1 of the high dose (50 mg/kg) samples used for D418 tumors. DLS intensity distributions, peaks, PDI, and % intensity for treatments 1–5 are shown in Supplementary Information; Supplementary Fig. S1. **B**, Schematic representation, drawn to scale, of an NSPT. The core is represented as an isotropic liquid or solid amorphous material of niclosamide stearate with a lipid monolayer of DSPC:cholesterol (45:50 mol:mol) providing a mechanical barrier to water penetration and protein binding, and a 5 mol% of DSPE-PEG²⁰⁰⁰ providing a steric barrier to protein binding around the niclosamide stearate core that is depicted here as an amorphous core (it may instead be crystalline, but that is yet to be fully confirmed). Also shown are the dimensions of each of the chemical structures (van der Waals surface) and size of the components, DSPC (3.1 nm), cholesterol (1.9 nm), DSPE-PEG²⁰⁰⁰, (DSPE 3.1 nm), and PEG (3.6 nm), making a total size of 6.7 nm and niclosamide stearate (3.0 nm).

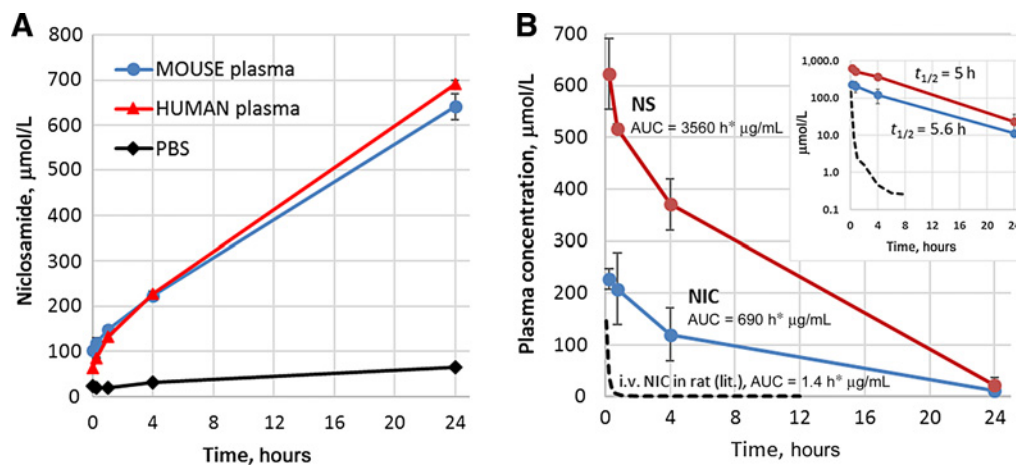
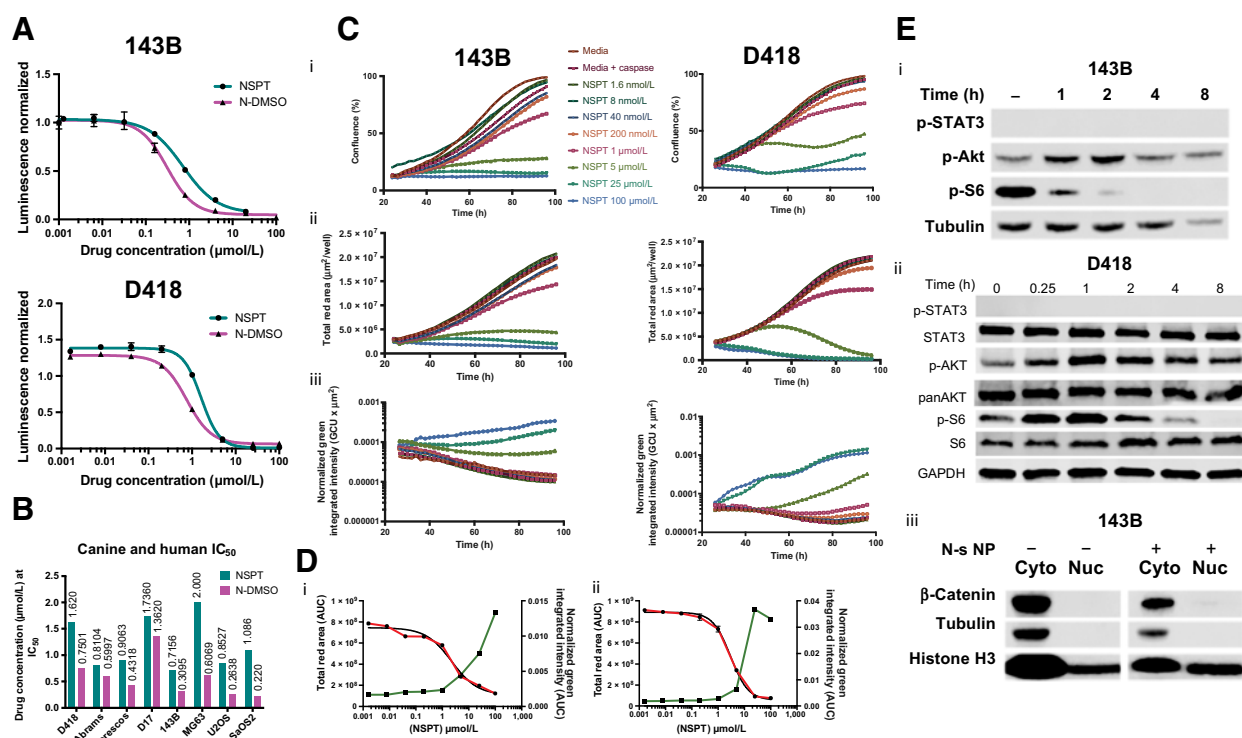


Figure 2.

In vitro stability and pharmacokinetics of the NSPT. **A**, Concentration of niclosamide (NIC) generated by hydrolysis and/or enzymolysis of niclosamide stearate (NS) core within NSPT (lipid-coated nanoparticles) in PBS, ($t_{1/2} = 17$ days) and mouse and human plasma ($t_{1/2} > 24$ hours) measured versus time for 0.25, 1, 4, and 24 hours at 37°C, starting with 1.8 mmol/L niclosamide stearate as NSPT. This is equivalent to the estimated zero time plasma concentration *in vivo* after bolus administration of dose of 50 mg/kg NSPT (27 mg/kg niclosamide equivalent). **B**, Concentration of niclosamide stearate and niclosamide in plasma measured over 24 hours after intravenous (i.v.) administration of 50 mg/kg NSPT (27 mg/kg niclosamide equivalent). The AUCs are: niclosamide stearate, 3,560 $\text{h} \cdot \mu\text{g/mL}$; and niclosamide, 690 $\text{h} \cdot \mu\text{g/mL}$. Plotted also are published niclosamide dosed intravenously at 2 mg/kg by dissolving the niclosamide in a mixture of DMSO/cremophor EL/water (3/15/82 v/v/v) in rat data (dashed) for illustration purposes (Chang and colleagues 2006) showing an AUC of only 1.4 $\text{h} \cdot \mu\text{g/mL}$ and a half-life of 6.7 ± 2.0 hours. Inset is the log-linear plot illustrating the similar half-life for both niclosamide stearate (5 hours) and niclosamide (5.5 hours) by a single-order decay.

Reddy et al.

**Figure 3.**

In vitro cell viability, proliferation, apoptosis, and Western blots. **A**, Dose-response assays for niclosamide in DMSO and NSPTs in canine osteosarcoma cell lines: 143B and D418 (see Supplementary Fig. S2A for individual plots of all eight cell lines). **B**, Cumulated IC_{50} values for all human (143B, MG63, U2OS, and SaOS2) and canine (D417, Moresco, Abrams, and D17) cell lines by treatment. **C**, Time- and dose-response assays of NSPTs on NLS mCherry-labeled 143B human and D418 canine osteosarcoma cells, representing: phase confluence % (i); red object fluorescence cell count (ii); and green object fluorescence area (iii) representative of caspase 3/7-dependent apoptotic events (see Supplementary Fig. S2B and S2C for individual plots of all eight cell lines). **D**, Cross-plots for 143B (i) and D418 (ii) of total red area and normalized green fluorescent intensity versus NSPT concentration at 96 hours (see Supplementary Fig. S2D for individual plots of all eight cell lines). **E**, Western blot signaling pathway analysis performed on human osteosarcoma cell line 143B (i) and patient-derived canine xenograft (D418) cells (ii) were incubated with 20 $\mu\text{mol/L}$ NSPTs for 0–8 hours. (iii), Western blots performed on the 143B cell line after no treatment or treatment with niclosamide stearate nanoparticles (20 $\mu\text{mol/L}$) for 24 hours (see Supplementary Fig. S3A and S3B for individual plots of all eight cell lines). Cell lysates were separated into cytoplasmic (Cyto) and nuclear (Nuc) fractions using Thermo Fisher Scientific's NE-PER Kit and samples were run on 4%–12% BT gels, transferred to polyvinylidene difluoride membranes and stained with antibodies to β -catenin, tubulin (cytoplasmic loading control), and Histone H3 (nuclear loading control).

and D418 canine osteosarcoma cells. **Figure 3C** (i) compares cell count and cell area representing phase confluence %. Below, about, 5 $\mu\text{mol/L}$ NSPT, cells showed increasing confluence and hence proliferation as total red area (**Fig. 3C**, ii). Above 5 $\mu\text{mol/L}$ there was a marked dose-dependent inhibition in cell proliferation in both cell lines. When plotted in **Fig. 3D**, the micromolar IC_{50} of NSPTs for this live cell imaging assay of proliferation (**Fig. 3A**) were similar to the IC_{50} for the cell viability (ATP-based endpoint) assay. **Figure 3C** (ii) for canine osteosarcoma cells (mean IC_{50} proliferation 3.46 $\mu\text{mol/L}$ vs. mean IC_{50} viability: 1.27 $\mu\text{mol/L}$, respectively; $P = 0.009$), but were somewhat greater for human (mean IC_{50} proliferation: 6.74 $\mu\text{mol/L}$ vs. mean IC_{50} viability: 0.88 $\mu\text{mol/L}$, respectively; $P = 0.17$). The green fluorescence intensity assay (**Fig. 3C**, iii) measured the response of the cells to NSPTs in terms of effective apoptosis. Here, the EC_{50} s of NSPTs on caspase 3/7-facilitated apoptosis in both 143B and D418 osteosarcoma cells showed clear evidence of apoptosis in a dose-dependent manner (see Supplementary Fig. S2B and S2C for individual plots of all eight cell lines).

As shown in the cross plots in **Fig. 3D**, cell proliferation was inhibited with increasing NSPT addition and the level of measured

apoptosis rose. The EC_{50} s for apoptosis although were significantly higher than the IC_{50} s for inhibition of proliferation (mean EC_{50} apoptosis: 20.9 $\mu\text{mol/L}$ vs. mean IC_{50} proliferation: 4.868 $\mu\text{mol/L}$; $P = 0.04$; see Supplementary Fig. S2D for individual plots of all eight cell lines). Time-dependent inhibition of proliferation by NSPTs was noted as quickly as 4 hours after initiation of treatment in the relatively high concentration, 100 $\mu\text{mol/L}$, groups. In these same high concentration, 100 $\mu\text{mol/L}$, groups caspase 3/7-mediated apoptosis was first noted 12 hours after initiation of treatment. Thus, there appears to be a slight nonapoptotic, cytotoxic inhibition of osteosarcoma cells when treated with lower concentrations and at earlier exposure times. The results of the Western blots are shown in **Fig. 3E** for both cell lines, as presented next.

NSPTs inhibited multiple human and canine osteosarcoma signaling pathways

Multiple signaling pathways have been implicated in niclosamide's growth inhibition of human and canine osteosarcoma cells, including NF- κ B, Wnt/ β -catenin, Notch, ROS, mTORC1, and Stat3, and so we expected, and tested to determine whether and to what extent NSPTs

would do the same (18). The PI3K/Akt/mTOR/S6 signaling pathway, and particularly the downstream mTOR and complex (mTORC1), are important regulators of cell-cycle progression and are frequently abnormally activated in osteosarcoma (65). Increasing mTOR activity has been shown to drive cell-cycle progression and increase cell proliferation. Conversely, as was shown in cervical cancer cells, the inhibition of mTOR (by the inhibitor AZD8055, at only 10 nmol/L) inhibits proliferation and glycolysis, and, again, was found to induce apoptosis in the HeLa cells in a time-dependent manner (66). In the same study by Li and colleagues, the phosphorylation of the C1 substrates p70S6K and phosphorylation of the mTORC2 substrate Akt were deregulated (66). An inhibition of mTOR in osteosarcoma cells could therefore correlate with their reduced proliferation (Fig. 3C). As shown in Fig. 3E, in both (i) 143B and (ii) D418, NSPTs induced a time-dependent reduction in the phosphorylated form of S6. Notably, in the D418 cell line, an initial increase in the p-Akt signal was observed at 1 hour before the signal decreased. The nuclear localization of β -catenin (Fig. 3E, iii) was reduced in separate cell lysates in 143B using nuclear/cytoplasmic fractionation of untreated and treated cells. The presence of nuclear β -catenin was also reduced in the 143B cell lines after 24 hours of treatment with 20 μ mol/L niclosamide stearate nanoparticles. As shown in Supplementary Fig. S3A and S3B for individual plots of all eight cell lines, nuclear β -catenin was also reduced in MG-63, U2OS, and SaOS2 cell lines after the same 24 hours of treatment with NSPT.

Taking all eight cell lines into consideration (see Supplementary Fig. S3A and S3B for individual plots of all eight cell lines), the amount of phosphorylated Akt did not change over 8 hours in Abrams and Moresco cell lines. As with the 143B and D418 lines, NSPTs also induced a time-dependent reduction in the phosphorylated form of S6 in MG-63, U2OS, SaOS2, D17, and Moresco. Phosphorylated STAT3 increased initially in MG-63, U2OS, SaOS2, and D17 before decreasing at 8 hours, while it was not present at all in the other human and canine osteosarcoma cells (see Supplementary Fig. S3A and S3B). Niclosamide's inhibition of the Akt/mTOR/S6 pathway is particularly beneficial, as mTOR/p70S6K has been clinically prognostic of disease-free and overall survival in patients presenting with primary osteosarcoma (67). Regarding the PI3K/Akt/mTOR/S6 pathway, NSPTs increased phosphorylated Akt but only transiently over the first 2 hours.

NSPTs decreased *ex vivo* growth of pulmonary metastases

To interrogate the ability of NSPTs to slow the progression of pulmonary metastases in 143B human and D418 canine osteosarcoma cells, we performed an *ex vivo* PuMA (60, 61). See also Supplementary Fig. S4 for images of lung slices loaded with osteosarcoma cancer cells prepared *ex vivo* after tracheotomy, as well as bright field fluorescence images of lung metastases in the lung tissues *ex vivo* on day 1 (400 ms exposure) at 5 \times magnification and a higher magnification (40 \times) image of fluorescence lung metastases. PBS control, doxorubicin, or NSPTs were administered to the lung slices upon plating out on the day of surgery. The fluorescence results of the PuMA (quantified as mean fluorescence area/total lung area) are shown in Fig. 4. For the PBS controls, both 143B and D418 cells established bulky, metastatic disease by day 5 and continued to develop through day 10.

Interestingly, the tumor burden was more prevalent at the initial stages (days 1 and 5) in the 143B human cell line, as quantified in Fig. 4B, than in the D418 canine, as quantified in Fig. 4D. For example, on days 1 and 5 the 143B human cell line showed increasing tumor burden of 0.018 and 0.042, while, in contrast the D418 tumor

burden started out at 0.0125 on day 1, and only increased slightly to 0.014 on day 5. However, while the 143B on day 10 had actually reduced slightly to 0.035, the D418 line increased dramatically to 0.06 by day 10.

For the drug-treated slices, all dosing (doxorubicin and NSPTs) was, as expected, relatively ineffective on day 1. Satisfyingly, NSPTs, at both 10 and 50 μ mol/L, were able to completely reduce the lung tumor burden to undetectable by day 5 in both 143B human (Fig. 4A–C) and D418 canine (Fig. 4D–F) osteosarcoma cells. The standard-of-care chemotherapeutic, doxorubicin, also significantly inhibited lung tumor burden at 1 and 10 μ mol/L concentrations, although, morphologically and quantitatively, there was a higher tumor burden in both cell lines at day 5 (Fig. 4B and C, D and F, respectively). By day 10, NSPTs continued to show complete reduction of tumor burden with no evidence of recovery, and the doxorubicin response had become morphologically and quantitatively similar to NSPT.

Thus, in the *ex vivo* PuMA we found that the assay accurately recreated the growth of 143B human and D418 canine osteosarcoma cells (which we had seen for controls in cell culture media as proliferation; Fig. 3C,i), but now within an actual lung tumor microenvironment. They also effectively showed the inhibitory effects of NSPTs when dosed in the culture dish medium through 1- to 2-mm thick lung parenchyma. Interestingly, the amounts of NSPTs that were effective in both 143B and D418 cell lines in the PuMA, when related to the IC_{50} s for cell viability from cell culture (0.71 and 1.6 μ mol/L), showed that NSPTs (10 μ mol/L by day 5) were able to massively inhibit the growth of pulmonary metastases in this model at only 14 \times and 6 \times the IC_{50} , for cell viability (ATP inhibition), respectively.

NSPTs administration to determine toxicity

The first feasibility study was carried out at a modest 0.59 mg/kg and no deleterious effects were seen in the mice in terms of toxicity or regarding weight loss over the first 30 days (Fig. 5D), until they succumbed to the lung metastases. We therefore decided to increase the dose and provide some measure of an MTD by carrying out a dose escalation and observing any response in C57BL/6 mice over 24 hours. As shown in Table 1, parameters for dose escalation study, three dosing levels were tested. The initial plasma concentrations achieved in the mice were not measured, but were calculated on the basis of a mouse blood volume of 1 mL (68, 69).

An NSPT injection into a C57BL/6 mouse of 100 μ L of a 1 mmol/L suspension concentration (equivalent to a 3.21 mg/kg dose and 91 μ mol/L NSPT in the blood stream), produced no changes in behavior when followed for 24 hours after injection. Similarly, increasing the 100 μ L injection concentration to a 6 mmol/L suspension of NSPTs (providing \sim 20 mg/kg and a blood concentration of 541 μ mol/L), also showed no adverse effects during 24-hour inspection in the 3 C57BL/6 mice. Because 6 mmol/L NSPTs was a relative upper concentration limit to our preparation at the time (including ultrafiltration for up-concentration), to achieve a higher dose, 200, 250, and 250 μ L were injected into each of 3 subsequent mice (to give 36.81, 45.77, and 47.24, equivalent to blood concentrations of 0.99, 1.19, and 1.19 mmol/L, respectively). Again, there were no adverse effects at 24 hours.

Therefore, the MTD was apparently not reached even at 50 mg/kg with up to 1.19 mmol/L of the prodrug niclosamide stearate (and therefore niclosamide) in the blood stream. We, therefore, used this much higher dose for the second metastatic assay experiment. The result was NSPTs can be administered to mice at 50 mg/kg without discernable toxicity.

Reddy et al.

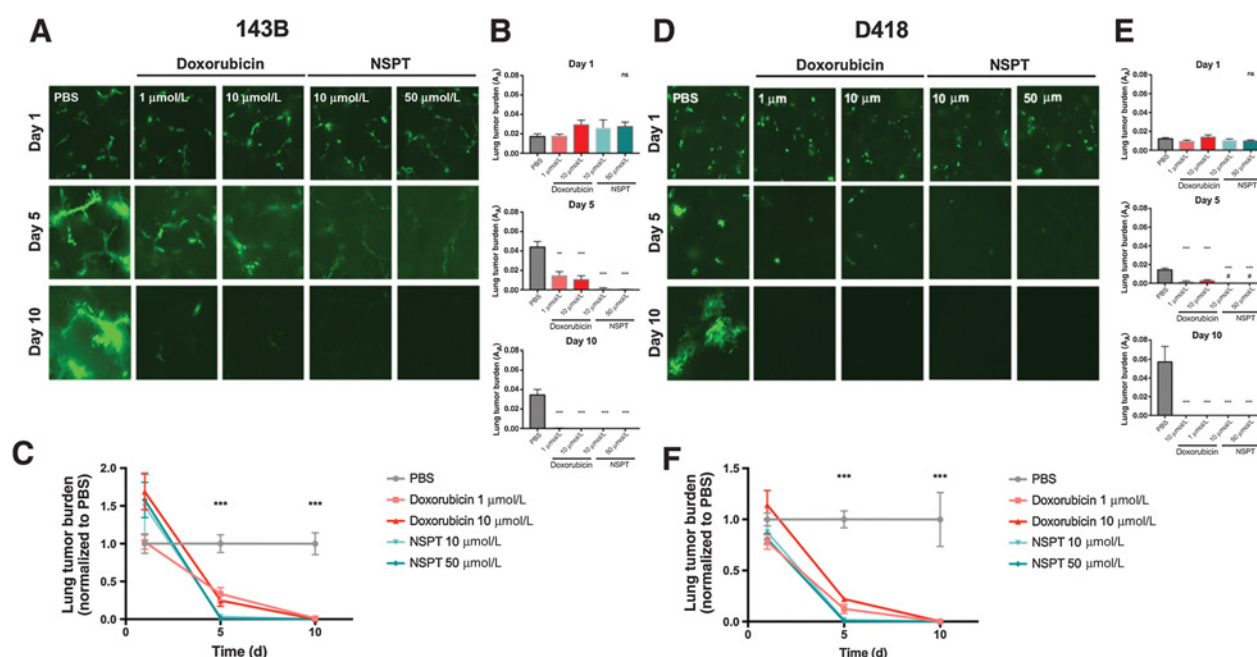


Figure 4.

The *ex vivo* PuMA. Representative fluorescence images of PuMA at 5 \times magnification with BF and EGFP filter sets in human 143B (A) and in canine D418 (D) from days 1, 5, and 10 following exposure to PBS, doxorubicin, and NSPTs. Exposure time was determined daily by PBS control fluorescence intensity. Dosing was done on the first day. Quantification of lung tumor burden in 143B (B) and in D418 (E) using mean fluorescence area over total lung area. Time-dependent change in treatment group. Lung tumor burden normalized to daily PBS lung tumor burden for 143B (C) and D418 (F). Note: these graphs represent normalized lung tumor burden. They are normalized to PBS lung tumor burden for each timepoint. The treatment groups are always referenced to that day's PBS that is why the PBS graph appears not to change while the treatment decreases. ns, not significant; **, $P < 0.01$ versus PBS; ***, $P < 0.001$ versus PBS; #, $P < 0.05$ versus doxorubicin 10 $\mu\text{mol/L}$.

***In vivo* studies at two dosings in a mouse model of osteosarcoma metastasis**

Two dosings of NSPTs were trialed. The first dose was at 0.59 mg/kg and was used as a safe and exploratory feasibility study of the possible effects of the new NSPTs in the lung metastasis model (70). Following the dose escalation study, where we had determined that a 50 mg/kg dose could be achieved without any discernable toxicity (and so was not even yet the MTD), the second study was carried out at this dose of 50 mg/kg NSPTs. To simulate the effect of metastatic disease, mice were inoculated via tail-vein injection with 5×10^5 luciferase-labeled 143B human or D418 canine PDX-derived osteosarcoma cells (as depicted schematically in Fig. 5E). This injection produced a colonization of the lung with osteosarcoma cells as disseminated metastases. Data for each study are now presented below.

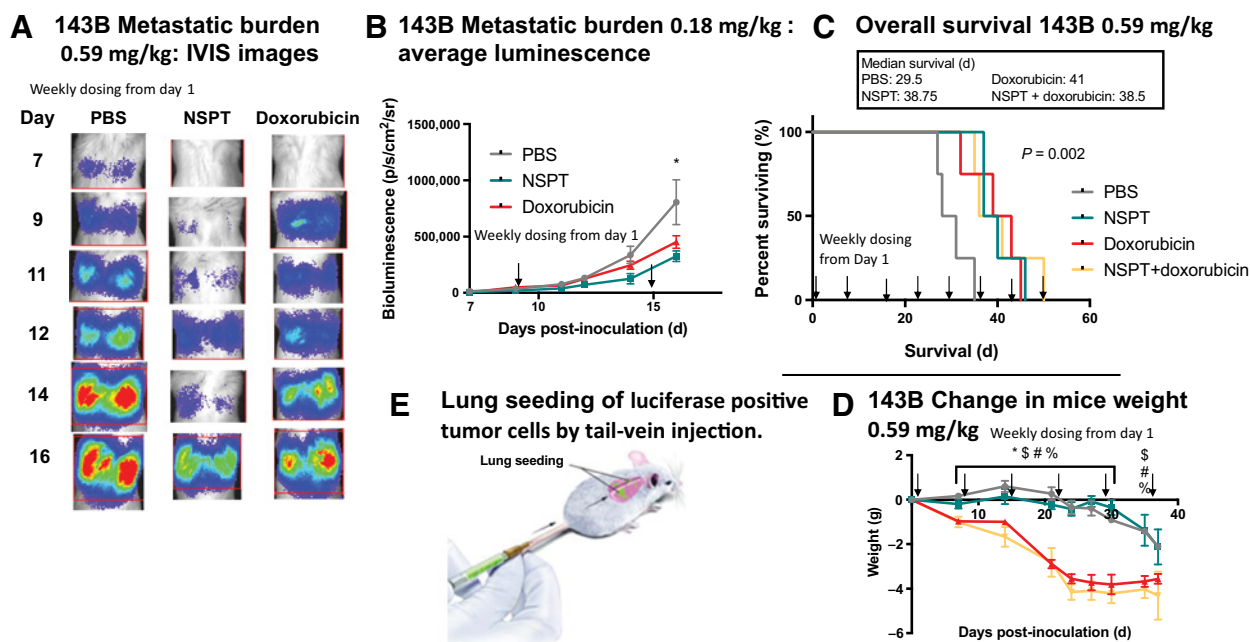
NSPTs at 0.59 mg/kg low-dose study

NSPTs at 0.59 mg/kg prolonged the survival in 143B-bearing mice without the treatment-derived morbidity shown by doxorubicin. In the low-dose study, a cohort of 16 12-week-old SCID/beige mice bearing the 143B tumor line were treated in groups with either weekly intravenous doses of: the control, 200 μL PBS; or 200 μL doses of niclosamide stearate nanoparticles in PBS suspension at a molar concentration of 100 $\mu\text{mol/L}$ (0.059 mg/mL); or weekly intraperitoneal doses of doxorubicin at 1.2 mg/kg in PBS; or combination therapy (niclosamide stearate nanoparticles intravenously weekly, doxorubicin intraperitoneally weekly). As shown in Fig. 5, they were followed for 50 days for overall survival, and for

17 days using IVIS imaging to observe and quantitate tumor burden. Mice were euthanized when they presented with signs of significant morbidity, such as lethargy or behavioral changes due to the lung metastatic burden. IVIS images in Fig. 5A, representing a typical example of the results, showed that the PBS control mice rapidly developed lung metastases within 7 days, and by day 16 there was massive lung tumor burden visible.

In contrast, both NSPT- and doxorubicin-treated mice showed reduced tumor burden compared with these controls. However, the NSPT cohort showed consistently less tumor burden than the doxorubicin-treated cohort. This visual data are quantified in Fig. 5B, giving the tumor burden as average bioluminescence in units of radiance “photons/second/cm²/steradian” (p/s/cm²/sr; see footnote¹). The doxorubicin and NSPT cohorts had a lower bioluminescence than controls with NSPTs being the least, signifying their lower tumor burden out to day 17. Thus, in mice that were inoculated with the human 143B cell line, treatment with niclosamide stearate nanoparticles at this first dose of 0.59 mg/kg was associated with delayed tumor

¹As described by Caliper Life Sciences Inc, 74. Sciences, C.L. *Image Display and Measurement*. 2011 9th February, 2019; Available from: <https://mbi-ctac.sites.medinfo.ufl.edu/files/2017/02/Concept-Tech-Note-2-Image-Display-and-Measurement.pdf>,” the radiance unit of photons/sec/cm²/sr is the number of photons per second that leave a square centimeter of tissue and radiate into a solid angle of one steradian (sr). A steradian can be thought of as a three-dimensional cone of light emitted from the surface that has a unit solid angle. Much like a radian is a unit of arc length for a circle, a steradian is a unit of solid angle for a sphere. An entire sphere has 4 π steradians. Lens systems typically collect light from only a small fraction of the total 4 π steradians.

**Figure 5.**

Low dose (0.59 mg/kg) *in vivo* study. Six-week-old SCID/beige mice were inoculated on day 0 with luciferase-labeled 143B (5×10^5) osteosarcoma cells and treated with 0.59 mg/kg weekly starting on day 1. Animals were injected weekly with 200 μ L of PBS or 200 μ L of a 100 μ mol/L suspension NSPTs, or doxorubicin, weekly at 1.2 mg/kg in PBS intraperitoneally. **A**, Luminescent images for PBS, NSPT, and doxorubicin versus time in a typical example. **B**, Average bioluminescence tumor burden in units of p/s/cm²/sr for each treatment group versus days post-inoculation for the first 17 days (error bars indicate SE). **C**, Kaplan–Meier survival curves for each treatment group with log-rank test comparing PBS, NSPT, doxorubicin, and combination therapy (NSPT + doxorubicin). Mice were also observed for signs of adverse effects including anorexia, dehydration, dyspnea, diarrhea, lethargy, or decreased grooming activity. **D**, Average change in weight by treatment group versus days post-inoculation for the first 39 days. **E**, Schematic showing how luciferase-positive tumor cells were delivered to mice by tail-vein injection, adapted from Mendoza and colleagues (60). Statistical significance: *, $P < 0.05$ versus PBS; #, $P < 0.05$ versus doxorubicin; \$, $P < 0.05$ PBS versus doxorubicin; #, $P < 0.05$ PBS versus NSPT + doxorubicin; %, $P < 0.05$ PBS versus NSPT + doxorubicin.

growth compared with the saline-treated group, with significantly less tumor burden at 14 and 16 days ($P = 0.0367$ and $P = 0.020$, respectively). Note: this 0.59 mg/kg dose represents a calculated blood concentration (based on a mouse weight of 20 g and a 1 mL mouse blood volume) of 20 μ mol/L; this is 12 \times the measured cell viability IC₅₀ (of 1.68 μ mol/L) for this 143B cell line from Fig. 3 (see later in Discussion).

In the Kaplan–Meier analysis (Fig. 5C), at the point at which all the PBS control mice had died, NSPT-treated mice were still at 100% survival. The 0.59 mg/kg NSPT treatment, given only on a weekly basis, prolonged survival with a mean survival of 40 days compared with 30 days in the PBS group ($P = 0.0067$; Fig. 5C). There was actually no statistically significant difference in survival between the mice treated with niclosamide stearate nanoparticles, doxorubicin, or combined therapy. Importantly, although for 143B human cell line, unfortunately, mice had to be euthanized early for the doxorubicin cohort. The doxorubicin-treated mice developed diarrhea and weight loss early in the course of therapy (Fig. 5D) and doxorubicin treatment was held for both doxorubicin-only and combined therapy groups at day 21. The NSPT- and PBS-treated groups did not demonstrate any early treatment-related side effects or weight loss out to at least 30 days, until they succumbed to cancer.

NSPTs at 50 mg/kg high-dose study

NSPTs at 50 mg/kg inhibited metastatic development in D418-bearing mice and safely delayed tumor progression. In this higher dose

study, 6-week-old SCID/beige mice were again inoculated via tail-vein injection with luciferase-labeled D418 canine PDX-derived osteosarcoma cells (as shown schematically in Fig. 5E). See Supplementary Table S1 for details of each mouse in the study, showing mouse weight (g), NPST diameter (nm), suspension concentration (mmol/L), and amount (mg) of NPST injected in each 200 μ L to achieve 50 mg/kg niclosamide stearate (equivalent to 27 mg/kg niclosamide) per mouse dosing.

Animals were treated with either the control of PBS or NSPTs by intravenous injection, or doxorubicin intraperitoneally. In this experiment, mice were relocated in the microscopy suite and so bioluminescence by IVIS was measured from day 0. As shown in Fig. 6B, immediately following inoculation, osteosarcoma cells were seen to be trapped in the lungs and gave an initial seeding bioluminescence that was not significantly different between treatment groups.

The seeding value decreased rapidly in PBS controls from $34,525 \pm 24,796$ p/s/cm²/sr value to $1,766 \pm 535$ p/s/cm²/sr at day 3, presumably, as cancer cells failed to survive and colonize. From day 10, although, the bioluminescence and hence tumor burden rapidly increased reaching levels of 30,000 p/s/cm²/sr, but now represented established metastases in the lungs. Interestingly, based on the IVIS images, in contrast to the 143B experiment (Fig. 5A), control mice inoculated with the same number (5×10^5 luciferase labeled) of D418 osteosarcoma cells took longer to develop the lung metastases (compare Fig. 5A day 16 with Fig. 6A day 17).

Reddy et al.

Table 1. Parameters for dose escalation study.

	Dose 1		Dose 2			Dose 3		
	Mouse 1	Mouse 1	Mouse 2	Mouse 3	Mouse 1	Mouse 2	Mouse 3	
Concentration injected NSPT, mmol/L	1	6	6	6	6	6	6	
Concentration injected NSPT, mg/mL ^a	0.59	3.53	3.53	3.53	3.53	3.53	3.53	
Injection volume, mL	0.1	0.1	0.1	0.1	0.2	0.25	0.25	
Mouse weight, g	18.5	17	17.5	18	19.2	19.3	18.7	
Injected NSPT mg/mouse	0.06	0.35	0.35	0.35	0.71	0.88	0.88	
Injected dose, mg/kg	3.21	20.79	20.19	19.63	36.81	45.77	47.24	
Blood concentration, $\mu\text{mol/L}^b$	90.91	541.17	541.17	541.17	992.14	1190.56	1190.56	

Note: The concentration that the injected dose achieves in the C57BL/6 mouse in units of $\mu\text{mol/L}$ is calculated based on a 1 mL mouse blood volume. Actual plasma volumes/mouse were based on 60 mL/kg, and so were 1.08, 0.99, 1.02, 1.05, 1.12, 1.13, and 1.09 mL (68, 69).

^aCalculated on the basis of 593.58 g/mol molar mass of niclosamide stearate.

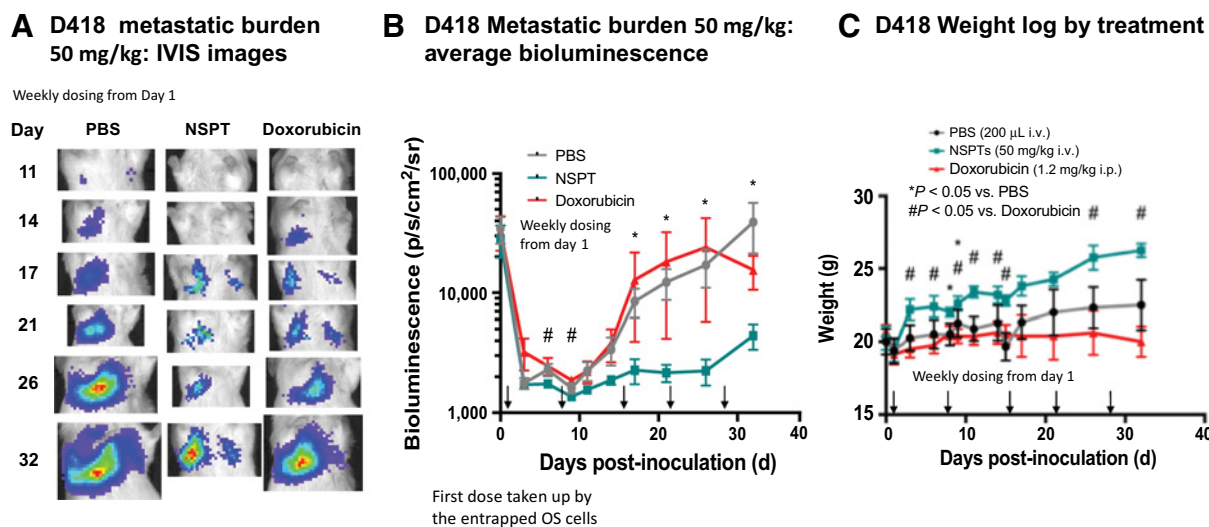
^bCalculated on the basis of a mouse blood volume of 1 mL.

Importantly, as shown in **Fig. 6B**, the lung tumor burden for mice treated with the NSPTs on only a weekly basis (days 1, 8, 15, 22, and 29), began to diverge from the PBS group at day 9, and remained at the approximately 2,000 p/s/cm²/sr bioluminescence baseline level out to 26 days, before rising slightly by the endpoint at day 32. This demonstrated for the first time that weekly dosing of NSPTs at 50 mg/kg prevented the establishment and controlled the metastatic disease in the lungs of the D418 cells. The result was even more significant in view of the data that showed this particular tumor was actually resistant to the standard-of-care drug, doxorubicin (**Fig. 6B**). Again, as with the lower 0.59 mg/kg dose cohort, NSPT-treated mice at 50 mg/kg did not have any weight loss associated with five weekly doses. Importantly, this drug (niclosamide) that has been shown to be relatively nontoxic in cell studies to healthy cells, even at this relatively large intravenous 50 mg/kg dose, NSPT-treated mice had significantly greater body weight when compared against doxorubicin-treated

mice, as shown in **Fig. 6C**, and even gained weight while on the dosing regimen.

Discussion

Taken together, our data suggest NSPT is a novel and effective formulation of niclosamide ready to undergo further evaluation as a new treatment for osteosarcoma. Analysis of the potential mechanism of action of this NSPT pinpointed multiple pathways known to be deregulated in osteosarcoma. Interestingly, other literature, as well as our own data *in vitro* indicate niclosamide, at its most fundamental level, acts by disrupting ATP synthesis (55, 71–74). As such, this mechanism acts upstream of many of the other processes in the osteosarcoma cell because they require ATP and phosphorylation to operate. Mechanistically, from a medicinal chemistry point of view, this activity of niclosamide represents a drug target that is not the usual

**Figure 6.**

High doses (50 mg/kg) *in vivo* study. Six-week-old SCID/beige mice were inoculated on day 0 with 5×10^5 luciferase-labeled D418 osteosarcoma cells and treated with 100 μL of PBS, 100 μL of a (e.g.) 8.44 mmol/L suspension of NSPTs dosed weekly, starting on day 1 or intraperitoneal (i.p.) doxorubicin, 1.2 mg/kg (MTD) weekly. **A**, Luminescent images for PBS, NSPT, and doxorubicin versus day after inoculation (note: first dose taken up by the entrapped osteosarcoma cells). **B**, Average bioluminescence tumor burden for each treatment group versus time (gray, PBS; red, doxorubicin; teal-green, NSPT) with error bars indicating SE. **C**, Average change in weight by treatment group versus days post-inoculation for the first 32 days. Mice were also observed for signs including anorexia, dehydration, dyspnea, diarrhea, lethargy, or decreased grooming activity. i.v., intravenous.

drug-protein (or -DNA, -RNA) macromolecule, but may instead represent activity at the lipid membrane level. In support of this hypothesis, niclosamide has been described as a proton shunt in mitochondria, and these effects induce osteosarcoma cell killing by apoptosis (71, 73). This brings into play a new kind of medicinal chemistry for drugability, that is, designing better lipophilic anions (a delocalized electron in relatively high logP-molecule) capable of even more efficient membrane partitioning and proton carrier functions to dissipate the pH gradients in mitochondria, lysosomes, and other internal cell organelles that rely on cation gradients.

Cell signaling studies for active components of the mTOR, Jak/STAT, and Wnt/ β -catenin pathways, showed that, in both human and canine osteosarcoma, NSPTs decreased the phosphorylated form of S6 (pS6) at 8 hours without any decrease in phosphorylated Akt. The PI3K/Akt/mTOR/S6 signaling pathway, and particularly the downstream mTOR and complex (mTORC1), are important regulators of cell-cycle progression and are frequently activated abnormally in osteosarcoma (65). Niclosamide's inhibition of the Akt/mTOR/S6 pathway is particularly beneficial, because mTOR functions as a sensor of mitogen, energy, and nutrient levels, and is a central controller of cell growth and a negative regulator of autophagy. The mTOR/p70S6K axis has been clinically prognostic of disease-free and overall survival in patients with primary osteosarcoma (67). In the D418 and D17 cell lines, while p-Akt was found to increase with treatment, the downstream decrease in p-S6 is likely due to direct inhibition of either mTORC1 or p70S6K.

In vivo, we observed significant reductions in metastatic burden and improved survival in mice with metastatic osteosarcoma at a low dose of just 0.59 mg/kg weekly. Following this positive "low-dose" data, we next used a dose of 50 mg/kg and found no increase in toxicity. While niclosamide itself when given orally is extremely safe, this is the first time that such a high dose of 50 mg/kg NSPT has been injected intravenously to obtain an initial dosing of 27 mg/kg equivalent niclosamide (34). For this particular drug, niclosamide and the pro-drug NSPTs, the issue is therefore not reducing toxicity, as it is in many chemotherapy applications, but more effective drug delivery (than oral dosing). Thus, in these experiments and with this NSPT design, the goal of bioavailable dosing had been achieved and, moreover, the NSPTs were efficacious in preventing metastatic disease without systemic toxicity.

When compared with the oral dosing in the clinical trial for prostate cancer of Schweizer and colleagues that gave sub-micromolar plasma concentrations that were not even close to the *in vitro* efficacy, our high-micromolar values are approximately 10,000 times the values achieved by oral dosing (36). Even in the prospective phase II clinical trial of niclosamide in patients with mCRC, the median C_{max} plasma levels of 0.665 $\mu\text{g/mL}$ ($\sim 2 \mu\text{mol/L}$), our values for NSPT are still almost 1,000 times the ones achieved with an oral dosing of 2 g/patient (40). This shows how extremely significant is of our new NSPT-based intravenous dosing approach to the cancer treatment by niclosamide.

We demonstrated here an innovative strategy to engage the principles of medicinal chemistry to repurpose an old, economical drug. We managed to optimize it for drug delivery as a unique nanoparticle formulation that increased the bioavailability of niclosamide in the blood stream (by intravenous injection of the prodrug at 50 mg/kg) and allowed its validation in the preclinical setting in mice with a well-performing lung metastasis model of osteosarcoma (75). Using bioluminescence tumor labeling, we were able to study and establish the *in vivo* efficacy of the NSPTs in both a human osteosarcoma cell line (143B) and a canine cell line (D418). The data suggest that 30-nm

diameter NSPTs are both effective and safe in treating simulated metastatic disease for both human and canine osteosarcoma in an *in vivo* mouse model. The NSPT nanoparticles were designed to be stable against hydrolysis due to the tight lipid-cholesterol monolayer, and "stealthy," that is, they contained enough DSPE-PEG²⁰⁰⁰ on their surfaces embedded in the DSPC:cholesterol monolayer that coated the particle to provide a relatively long (6–7 hours) circulation half-life for the prodrug compound. Currently, there are no other options for administering niclosamide intravenously preclinically except from a direct DMA injection (51), which is clinically unacceptable. Our prodrug delivery strategy converted the relatively water insoluble niclosamide ($S_w = 4 \mu\text{mol/L}$) to its even less soluble ($\sim 30 \text{ nmol/L}$) stearate ester for the expressed purpose of making injectable NSPT nanoparticles at doses at least as high as 50 mg/kg. This strategy has successfully transformed a previously unacceptably low-bioavailable niclosamide into a customizable and efficacious therapeutic with the requisite pharmacokinetics and tolerability profile for immediate canine and subsequent human clinical testing. NSPTs are able to inhibit osteosarcoma cell growth in several orthogonal modalities ($IC_{50} = 0.2\text{--}2 \mu\text{mol/L}$) and function as effective prodrug therapeutics in metastatic osteosarcoma *in vivo*, leading to decreased metastatic tumor burden *ex vivo* and *in vivo*. Future directions will be multilateral and involve several areas of interest. Perhaps the most important from a biological and interaction standpoint is further elucidating the broad mechanisms of NSPTs and indeed niclosamide on osteosarcoma cells and other solid tumors. In addition, this would be helpful in then determining an *in vivo* pharmacokinetic marker of NSPT action. Different nanoparticle formulations (ligand targeting, fluorescent tagging, active immunomodulation, etc.) and combinations with established and candidate chemotherapeutics and concentrations can be trialed in high-throughput *in vitro* and *ex vivo* PuMA screens. Validating a primary orthotopic model that can spontaneously metastasize would then provide another opportunity to test NSPTs' effectiveness in a complementary model. Finally, pilot clinical testing in canine patients with primary and metastatic osteosarcoma would provide valuable, actionable insight into the viability and challenges with NSPT production, drug quality assurance, and clinical administration and subsequent tolerability observations. From those early clinical studies, additional clinical studies can be escalated to larger canine, randomized control trials, and human phase I studies to realize the ultimate goals of improving survival and decreasing morbidity for patients with osteosarcoma.

Disclosure of Potential Conflicts of Interest

B.E. Brigman is a consultant (paid consultant) at Daiichi Sankyo, and is a member of medical board of directors at and reports receiving a commercial Research Grant from Musculoskeletal Transplant Foundation. No potential conflicts of interest were disclosed by the other authors.

Authors' Contributions

Conception and design: D.L. Kerr, A. Tovmasyan, B.E. Brigman, J.A. Somarelli, D. Needham, W.C. Eward

Development of methodology: G.B. Reddy, D.L. Kerr, I. Spasojevic, A. Tovmasyan, J.A. Somarelli, D. Needham, W.C. Eward

Acquisition of data (provided animals, acquired and managed patients, provided facilities, etc.): G.B. Reddy, D.L. Kerr, I. Spasojevic, A. Tovmasyan, J.A. Somarelli, W.C. Eward

Analysis and interpretation of data (e.g., statistical analysis, biostatistics, computational analysis): G.B. Reddy, D.L. Kerr, I. Spasojevic, A. Tovmasyan, J.A. Somarelli, D. Needham, W.C. Eward

Writing, review, and/or revision of the manuscript: G.B. Reddy, D.L. Kerr, I. Spasojevic, A. Tovmasyan, D. Hsu, J.A. Somarelli, D. Needham, W.C. Eward

Reddy et al.

Administrative, technical, or material support (i.e., reporting or organizing data, constructing databases): G.B. Reddy, D.L. Kerr, B.E. Brigman, D. Needham, W.C. Eward

Study supervision: J.A. Somarelli, D. Needham, W.C. Eward

Acknowledgments

This work was funded by a Hyundai Hope on Wheels Award.

The costs of publication of this article were defrayed in part by the payment of page charges. This article must therefore be hereby marked *advertisement* in accordance with 18 U.S.C. Section 1734 solely to indicate this fact.

Received July 11, 2019; revised November 17, 2019; accepted April 21, 2020; published first May 5, 2020.

References

- Friebele JC, Peck J, Pan X, Abdel-Rasoul M, Mayerson JL. Osteosarcoma: a meta-analysis and review of the literature. *Am J Orthop* 2015;44:547–53.
- Taran SJ, Taran R, Malipatil NB. Pediatric osteosarcoma: an updated review. *Indian J Med Paediatr Oncol* 2017;38:33.
- Biermann JS, Chow W, Reed DR, Lucas D, Adkins DR, Agulnik M, et al. NCCN guidelines insights: bone cancer, version 2.2017. *J Natl Compr Canc Netw* 2017; 15:155–67.
- Mialou V, Philip T, Kalifa C, Perol D, Gentet J-C, Marec-Berard P, et al. Metastatic osteosarcoma at diagnosis: prognostic factors and long-term outcome—the French pediatric experience. *Cancer* 2005;104:1100–9.
- Aljubran AH, Griffin A, Pintilie M, Blackstein M. Osteosarcoma in adolescents and adults: survival analysis with and without lung metastases. *Ann Oncol* 2009; 20:1136–41.
- Kager L, Zoubek A, Pötschger U, Kastner U, Flege S, Kempf-Bielack B, et al. Primary metastatic osteosarcoma: presentation and outcome of patients treated on neoadjuvant Cooperative Osteosarcoma Study Group protocols. *J Clin Oncol* 2003;21:2011–8.
- Mirabello L, Troisi RJ, Savage SA. Osteosarcoma incidence and survival rates from 1973 to 2004. *Cancer* 2009;115:1531–34.
- Crawford S. Is it time for a new paradigm for systemic cancer treatment? Lessons from a century of cancer chemotherapy. *Front Pharmacol* 2013;4:68.
- Kansara M, Teng MW, Smyth MJ, Thomas DM. Translational biology of osteosarcoma. *Nat Rev Cancer* 2014;14:722–35.
- Whelan JS, Bielack SS, Marina N, Smeland S, Jovic G, Hook JM, et al. EUR-AMOS-1, an international randomised study for osteosarcoma: results from pre-randomisation treatment. *Ann Oncol* 2014;26:407–14.
- Marina NM, Smeland S, Bielack SS, Bernstein M, Jovic G, Krailo MD, et al. Comparison of MAPIE versus MAP in patients with a poor response to preoperative chemotherapy for newly diagnosed high-grade osteosarcoma (EURAMOS-1): an open-label, international, randomised controlled trial. *Lancet Oncol* 2016;17:1396–408.
- Ferrari S, Ruggieri P, Cefalo G, Tamburini A, Capanna R, Fagioli F, et al. Neoadjuvant chemotherapy with methotrexate, cisplatin, and doxorubicin with or without ifosfamide in nonmetastatic osteosarcoma of the extremity: an Italian sarcoma group trial ISG/OS-1. *J Clin Oncol* 2012;30:2112–8.
- Nagarajan R, Kamruzzaman A, Ness KK, Marchese VG, Sklar C, Mertens A, et al. Twenty years of followup of survivors of childhood osteosarcoma. *Cancer* 2011; 117:625–34.
- Kadri H, Lambourne OA, Mehellou Y. Niclosamide, a drug with many (Re) purposes. *ChemMedChem* 2018;13:1088–91.
- Arend RC, Londoño-Joshi AI, Straughn JM, Buchsbaum DJ. The Wnt/ β -catenin pathway in ovarian cancer: a review. *Gynecol Oncol* 2013;131:772–9.
- Osada T, Chen M, Yang XY, Spasojevic I, Vandeusen JB, Hsu D, et al. Anthelmintic compound niclosamide downregulates WNT signaling and elicits antitumor responses in tumors with activating APC mutations. *Cancer Res* 2011;71:4172–82.
- Londoño-Joshi AI, Arend RC, Aristizabal L, Lu W, Samant RS, Metge BJ, et al. Effect of niclosamide on basal-like breast cancers. *Mol Cancer Ther* 2014;13: 800–11.
- Pan JX, Ding K, Wang CY. Niclosamide, an old anthelmintic agent, demonstrates antitumor activity by blocking multiple signaling pathways of cancer stem cells. *Chin J Cancer* 2012;31:178–84.
- Jin Y, Lu Z, Ding K, Li J, Du X, Chen C, et al. Antineoplastic mechanisms of niclosamide in acute myelogenous leukemia stem cells: inactivation of the NF- κ B pathway and generation of reactive oxygen species. *Cancer Res* 2010; 70:2516–27.
- Perera DR, Western KA, Schultz MG. Niclosamide* treatment of cestodiasis. *Am J Trop Med Hyg* 1970;19:610–2.
- Li Y, Li P-K, Roberts MJ, Arend RC, Samant RS, Buchsbaum DJ. Multi-targeted therapy of cancer by niclosamide: a new application for an old drug. *Cancer Lett* 2014;349:8–14.
- Ahmed K, Shaw H, Koval A, Katanaev V. A second WNT for old drugs: drug repositioning against WNT-dependent cancers. *Cancers* 2016;8:66.
- Chen M, Wang J, Lu J, Bond MC, Ren X-R, Lyrly HK, et al. The anti-helminthic niclosamide inhibits Wnt/Frizzled1 signaling. *Biochemistry* 2009; 48:10267–74.
- Suliman MA, Zhang Z, Na H, Ribeiro ALL, Zhang Y, Niang B, et al. Niclosamide inhibits colon cancer progression through downregulation of the Notch pathway and upregulation of the tumor suppressor miR-200 family. *Int J Mol Med* 2016; 38:776–84.
- Arslanagic A, et al. Characterization of targeted and non-targeted uptake in breast cancer stem cells of triple negative origin. In *CLINAM: Basel, Switzerland*; 2016.
- Arslanagic-Kabiljagic A. Establishing the feasibility for endogenous delivery of pure-drug anti-cancer nanoparticles in the treatment of metastatic breast cancer disease. In *Biochemistry and Molecular Biology*. University Southern Denmark, Copenhagen, Denmark; 2019.
- Karimi L. Preclinical Characterization and *In vitro* Cell testing of novel niclosamide nanoparticle formulations for treatment of prostate cancer. In *Biochemistry and Molecular Biology*, NY, NY; 2019.
- NCI. NCI DTP (Developmental therapeutics program), NCI 60 screening results. 2014; Available from: https://dtp.cancer.gov/services/nci60data/colorado_seresponse/jpg/758440.
- Li Z, Yu Y, Sun S, Qi B, Wang W, Yu A. Niclosamide inhibits the proliferation of human osteosarcoma cell lines by inducing apoptosis and cell cycle arrest. *Oncol Rep* 2015;33:1763–8.
- Park S-J, Shin J-H, Kang H, Hwang J-J, Cho D-H. Niclosamide induces mitochondria fragmentation and promotes both apoptotic and autophagic cell death. *BMB Rep*. 2011;44:517–22.
- Ye T, Xiong Y, Yan Y, Xia Y, Song X, Liu L, et al. The anthelmintic drug niclosamide induces apoptosis, impairs metastasis and reduces immunosuppressive cells in breast cancer model. *PLoS One* 2014;9:e85887.
- Liao Z, Nan G, Yan Z, Zeng L, Deng Y, Ye J, et al. The anthelmintic drug niclosamide inhibits the proliferative activity of human osteosarcoma cells by targeting multiple signal pathways. *Curr Cancer Drug Targets* 2015;15:726–38.
- Environmental Protection And Toxic Substances, Agency. Niclosamide 1999, United States Prevention, Pesticides EPA-738-F99-013, Environmental Protection And Toxic Substances, Agency (7508C). Available from: <https://archive.epa.gov/pesticides/reregistration/web/pdf/2455fact.pdf>.
- World Health Organization. WHO specifications and evaluations for public health pesticides: niclosamide. Geneva, Switzerland: World Health Organization; 2002.
- Ebbesen MF, BJ, Atalini P, Elie A, Needham D. Solubility of Niclosamide and its binding to albumin as a function of pH predicts uptake and accumulation in lysosomes and lipid droplets in cancer cell cultures. Podium Presentation, Duke Cancer Institute; 2019.
- Schweizer MT, Haugk K, McKiernan JS, Gulati R, Cheng HH, Maes JL, et al. A phase I study of niclosamide in combination with enzalutamide in men with castration-resistant prostate cancer. *PLoS One* 2018;13: e0198389.
- Liu C, Lou W, Armstrong C, Zhu Y, Evans CP, Gao AC. Niclosamide suppresses cell migration and invasion in enzalutamide resistant prostate cancer cells via Stat3-AR axis inhibition. *Prostate* 2015;75:1341–53.
- Morse M. A phase I study: A study of niclosamide in patients with resectable colon cancer (Pro00066964). Duke University Medical Center; 2017.
- Burock S, Daum S, Keilholz U, Neumann K, Walther W, Stein U. Phase II trial to investigate the safety and efficacy of orally applied niclosamide in patients with

Novel Nanoparticle Niclosamide Treats Osteosarcoma

- metachronous or synchronous metastases of a colorectal cancer progressing after therapy: the NIKOLO trial. *BMC Cancer* 2018;18:297.
40. Burock S, Daum S, Tröger H, Kim TD, Krüger S, Rieke DT, et al. Niclosamide a new chemotherapy agent? Pharmacokinetics of the potential anticancer drug in a patient cohort of the NIKOLO trial. *J Clin Oncol* 2018;36:e14536.
 41. Hervella P, Walke P, Arslanagic A, Azevedo C, Ulven T, et al. A new niclosamide stearate prodrug therapeutic of the re-appropriated anti-cancer drug niclosamide: formulation, size distribution, and chemical stability against hydrolysis and enzymolysis. *J Pharm Sci*. 2019;13:1088–91.
 42. Needham D, Arslanagic A, Glud K, Hervella P, Karimi L, Høeilund-Carlsen P-F, et al. Bottom up design of nanoparticles for anti-cancer diapeutics: "put the drug in the cancer's food". *J Drug Target* 2016;24:836–56.
 43. Walke P. Physico-chemical parameters of nanoparticles that govern prodrug design and application in anticancer nanomedicine. In *Physics, Chemistry, Pharmacy*. University of Southern Denmark (SDU); 2018.
 44. Walke PB, Hervella P, Needham D. Lipid-coated stealth nanoparticles of novel hydrophobic prodrug, niclosamide stearate, as cancer therapeutic: formulation and physico-chemical Characterization of nanoparticles. In 6th International Pharmaceutical Federation Pharmaceutical Sciences World Congress; May 21–24, 2017. Stockholm, Sweden.
 45. Mehta M. Biopharmaceutics classification system (BCS): development, implementation, and growth. Wiley, Hoboken, NJ, USA; 2016.
 46. Eward W. Testing a new prodrug nanoparticle formulation of niclosamide as a novel therapy for osteosarcoma. In: Consortium for Canine Comparative Oncology, the College of Veterinary Medicine at NC State University and the Duke Cancer Institute; 2018; Durham, NC.
 47. Misra SK, Wang X, Srivastava I, Imgruet MK, Graff RW, Ohoka A, et al. Combinatorial therapy for triple negative breast cancer using hyperstar polymer-based nanoparticles. *Chem Commun* 2015;51:16710–3.
 48. Bhushan B, Dubey P, Kumar SU, Sachdev A, Matai I, Gopinath P. Bionanotherapeutics: niclosamide encapsulated albumin nanoparticles as a novel drug delivery system for cancer therapy. *RSC Adv* 2015;5:12078–86.
 49. Jain NK, Srivastava R, Naidu V. Niclosamide loaded cationic solid lipid nanoparticles for treatment of Cancer. In: IEEE 16th International Conference on Nanotechnology (IEEE-NANO); 2016 Aug 22–25; Sendai, Japan.
 50. Zhirnik AS, Semochkina YP, Moskaleva EY, Krylov NI, Tubasheva IA, Kuznetsov SL, et al. Molecular mechanisms of antitumor activity of the polymeric form of niclosamide with respect to human colorectal cancer cells. *Biochemistry (Moscow), Supplement Series B: J Biomed Chem* 2017;11:301–7.
 51. Bhattacharyya J, Ren X-R, Mook RA, Wang J, Spasojevic I, Premont RT, et al. Niclosamide-conjugated polypeptide nanoparticles inhibit Wnt signaling and colon cancer growth. *Nanoscale* 2017;9:12709–17.
 52. Mook RA, Wang J, Ren X-R, Chen M, Spasojevic I, Barak LS, et al. Structure-activity studies of Wnt/ β -catenin inhibition in the Niclosamide chemotype: Identification of derivatives with improved drug exposure. *Bioorg Med Chem* 2015;23:5829–38.
 53. Ye Y, Zhang X, Zhang T, Wang H, Wu B. Design and evaluation of injectable niclosamide nanocrystals prepared by wet media milling technique. *Drug Dev Ind Pharm* 2015;41:1416–24.
 54. Dubey P, Gopinath P. Fabrication of electrospun poly(ethylene oxide)-poly (capro lactone) composite nanofibers for co-delivery of niclosamide and silver nanoparticles exhibits enhanced anti-cancer effects *in vitro*. *J Mater Chem B* 2016;4:726–42.
 55. Sukumar UK, Gopinath P. Field-actuated antineoplastic potential of smart and versatile PEO-bPEI electrospun scaffold by multi-staged targeted co-delivery of magnetite nanoparticles and niclosamide-bPEI complexes. *RSC Adv* 2016;6: 46186–201.
 56. Needham D, et al. Nucleation, growth and characterization of triolein nanoparticles prepared in the absence and presence of phospholipids by rapid solvent shifting technique. 2019.
 57. Zhigaltsev IV, Belliveau N, Hafez I, Leung AKK, Huft J, Hansen C, et al. Bottom-up design and synthesis of limit size lipid nanoparticle systems with aqueous and triglyceride cores using millisecond microfluidic mixing. *Langmuir* 2012;28: 3633–40.
 58. Tetko IV, Tanchuk VY. ALOGPS is a free on-line program to predict lipophilicity and aqueous solubility of chemical compounds. 2019. Available from: <http://www.vcclab.org/lab/alogps/>.
 59. Karthika S, Radhakrishnan TK, Kalaichelvi P. A review of classical and non-classical nucleation theories. *Cryst Growth Des* 2016;16:6663–81.
 60. Mendoza A, Hong S-H, Osborne T, Khan MA, Campbell K, Briggs J, et al. Modeling metastasis biology and therapy in real time in the mouse lung. *J Clin Invest* 2010;120:2979–88.
 61. Lizardo M, Sorensen P. Practical considerations in studying metastatic lung colonization in osteosarcoma using the pulmonary metastasis assay. *J Vis Exp* 2018;133:56332.
 62. Sebaugh JL. Guidelines for accurate EC50/IC50 estimation. *Pharm Stat* 2011;10: 128–34.
 63. Chang Y-W, Yeh T-K, Lin K-T, Chen W-C, Yao H-T, Lan S-J, et al. Pharmacokinetics of anti-SARS-CoV agent niclosamide and its analogs in rats. *J Food Drug Anal* 2006;14:329–33.
 64. Hervella P, Dam JH, Thisgaard H, Baun C, Olsen BB, Høeilund-Carlsen PF, et al. Chelation, formulation, encapsulation, retention, and *in vivo* biodistribution of hydrophobic nanoparticles labelled with ⁵⁷Co-porphyrin: Oleylamine ensures stable chelation of cobalt in nanoparticles that accumulate in tumors. *J Control Release*. 2018 Dec 10;291:11–25. doi: 10.1016/j.jconrel.2018.09.027. Epub 2018 Oct 3. PMID: 30291986.
 65. Ding L, Congwei L, Bei Q, Tao Y, Ruiguo W, Heze Y, et al. mTOR: an attractive therapeutic target for osteosarcoma? *Oncotarget* 2016;7:50805.
 66. Li S, Li Y, Hu R, Li W, Qiu H, Cai H, et al. The mTOR inhibitor AZD8055 inhibits proliferation and glycolysis in cervical cancer cells. *Oncol Lett* 2013;5:717–21.
 67. Zhou Q, Deng Z, Zhu Y, Long H, Zhang S, Zhao J. mTOR/p70S6K signal transduction pathway contributes to osteosarcoma progression and patients' prognosis. *Med Oncol* 2010;27:1239–45.
 68. Riches AC, Sharp JG, Thomas DB, Smith SV. Blood volume determination in the mouse. *J Physiol* 1973;228:279–84.
 69. NC3Rs. Decision tree. 2019; Available from: <https://www.nc3rs.org.uk/mouse-decision-tree-blood-sampling>.
 70. Kerr DL. A novel formulation of niclosamide treats metastatic osteosarcoma *in vivo*. Durham, NC: Duke University, School of Medicine; 2017.
 71. Alasadi A, Chen M, Swapna GVT, Tao H, Guo J, Collantes J, et al. Effect of mitochondrial uncouplers niclosamide ethanalamine (NEN) and oxyclozanide on hepatic metastasis of colon cancer. *Cell Death Dis* 2018;9: 215.
 72. Childress ES, Alexopoulos SJ, Hoehn KL, Santos WL. Small molecule mitochondrial uncouplers and their therapeutic potential. *J Med Chem* 2018;61:4641–55.
 73. Jurgeit A, McDowell R, Moese S, Meldrum E, Schwendener R, Greber UF. Niclosamide is a proton carrier and targets acidic endosomes with broad antiviral effects. *PLoS Pathog* 2012;8:e1002976.
 74. Park S-J, Shin J-H, Kang H, Hwang J-J, Cho D-H. Niclosamide induces mitochondria fragmentation and promotes both apoptotic and autophagic cell death. *BMB Rep* 2011;44:517–22.
 75. Chen W, Mook jr, Wang RA, Jiangbo R, Xiu-Rong C, Minyong B, et al. Chemical modulators of signaling pathways and therapeutic use, 2016. Available from: <https://olv.duke.edu/technologies/chemical-modulators-of-signaling-pathways-and-therapeutic-use/>.

Molecular Cancer Therapeutics

Preclinical Testing of a Novel Niclosamide Stearate Prodrug Therapeutic (NSPT) Shows Efficacy Against Osteosarcoma

Gireesh B. Reddy, David L. Kerr, Ivan Spasojevic, et al.

Mol Cancer Ther 2020;19:1448-1461. Published OnlineFirst May 5, 2020.

Updated version Access the most recent version of this article at:
doi:[10.1158/1535-7163.MCT-19-0689](https://doi.org/10.1158/1535-7163.MCT-19-0689)

Supplementary Material Access the most recent supplemental material at:
<http://mct.aacrjournals.org/content/suppl/2020/05/06/1535-7163.MCT-19-0689.DC2>
<http://mct.aacrjournals.org/content/suppl/2020/05/02/1535-7163.MCT-19-0689.DC1>

Cited articles This article cites 56 articles, 7 of which you can access for free at:
<http://mct.aacrjournals.org/content/19/7/1448.full#ref-list-1>

E-mail alerts [Sign up to receive free email-alerts](#) related to this article or journal.

Reprints and Subscriptions To order reprints of this article or to subscribe to the journal, contact the AACR Publications Department at pubs@aacr.org.

Permissions To request permission to re-use all or part of this article, use this link
<http://mct.aacrjournals.org/content/19/7/1448>.
Click on "Request Permissions" which will take you to the Copyright Clearance Center's (CCC) Rightslink site.